Substrate Binding and Catalysis of Ecto-ADP-ribosyltransferase 2.2 from Rat†

Holger Ritter,‡ Friedrich Koch-Nolte,§ Victor E. Marquez,|| and Georg E. Schulz*,‡

Institut für Organische Chemie und Biochemie, Albert-Ludwigs-Universität, Albertstrasse 21, Freiburg im Breisgau 79104, Germany, Institut für Immunologie, Universitätsklinikum Eppendorf, Martinistrasse 52, Hamburg 20246, Germany, and Laboratory of Medicinal Chemistry, Center for Cancer Research, NCI−Frederick, Frederick, Maryland 21702

Received April 21, 2003; Revised Manuscript Received July 3, 2003

ABSTRACT: The structures of β-methylenethiazole-4-carboxamide adenine dinucleotide (TAD), NAD^+, and NADH as bound to ecto-ADP-ribosyltransferase 2.2 from rat and to its mutants E189I and E189A, respectively, have been established. The positions and conformations of NAD^+ and its analogues agree in general with those in other ADP-ribosyltransferases. The kinetic constants for NAD^+ hydrolysis were determined by RP-HPLC. The specific activity amounts to 26 units/mg, which is 6000-fold higher than a previously reported rate and 500-fold higher than the hydrolysis rates of other ADP-ribosyltransferases, confirming that hydrolysis is the major function of this enzyme. On the basis of structures and mutant activities, a catalytic mechanism is proposed. The known auto-ADP-ribosylation of the enzyme at the suggested position R184 is supported by one of the crystal structures where the nucleophile position is occupied by an Nη atom of this arginine which in turn is backed up by the base E159.

ADP-ribosylation of proteins is an important posttranslational modification in which the ADP-ribosyl moiety of NAD^+ is transferred to a target molecule and nicotinamide is released (Figure 1). The ADP-ribosyltransferase (ART)[1] family comprises various virulence factors of prokaryotic pathogens that cause serious human diseases such as cholera or diphtheria (*1*, *2*). Nine structures of prokaryotic ARTs are known, all of which are toxins (*3*, *4*). The two known structures of eukaryotic ARTs represent the poly(ADP-ribosyl)polymerase (PARP) and the ecto-ART families that differ from each other appreciably (*5*, *6*). PARP is located in the nucleus and ADP-ribosylates itself and other nuclear proteins by attaching branched ADP-ribose polymers in multiple transfer reactions. The ecto-ART family is located in the extracellular space of mammalian tissues, comprising the four glycosylphosphatidylinositol- (GPI-) anchored proteins ART1−ART4 and the secretory protein ART5, some of which play a role in the immune system (*7*−*10*). This family is structurally closer related to some bacterial toxins than to PARP (*6*).

The functionally best characterized proteins of the ecto-ART family are mouse ART1 and ART2 that ADP-ribosylate members of the integrin family of adhesion molecules in vivo and arginine-rich histones as well as polyarginine in vitro (*11*, *12*). Moreover, it has been shown that mouse ART2 is involved in NAD^+-induced apoptosis (*13*−*15*). In contrast, the rat ecto-ADP-ribosyltransferase 2.2 (rART2.2), which is here analyzed, does not ADP-ribosylate cell surface proteins (*16*−*17*). This is probably due to an exchange at position 187 (Q187 in rat versus E187 in mouse) as Q187E mutants of the rat enzyme were able to modify target proteins at arginines (*18*−*20*). NAD^+ is a typical cytoplasmic substance

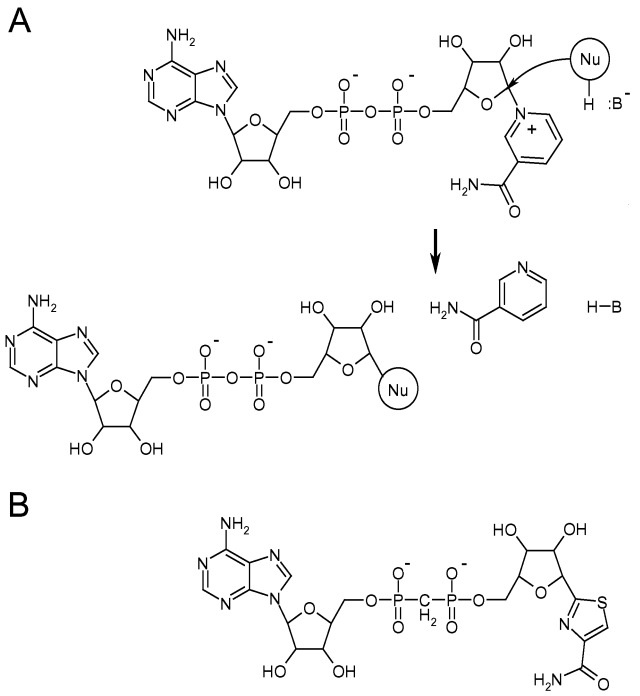

FIGURE 1: ART substrate and reaction. (A) Transfer of the ADP-ribosyl moiety of NAD^+ onto a nucleophile, which can be a water molecule (NAD^+ hydrolysis) or any other nucleophilic group. The nucleophile may release a proton to be picked up by a base. Nicotinamide is an excellent leaving group whereas NADH is not a substrate. (B) Inactive substrate analogue TAD.

† The project was supported by the Deutsche Forschungsgemeinschaft under SFB-388.

* Corresponding author. Tel: +49-761-203-6058. Fax: +49-761-203-6161. E-mail: schulz@bio.chemie.uni-freiburg.de.

‡ Albert-Ludwigs-Universität.

§ Universitätsklinikum Eppendorf.

|| NCI−Frederick.

[1] Abbreviations: ART, ADP-ribosyltransferase; rART2.2, ecto-ADP-ribosyltransferase 2.2 from rat (*Rattus norvegicus*); GPI, glycosylphosphatidylinositol; PARP, poly(ADP-ribosyl)polymerase; RP-HPLC, reversed-phase high-performance liquid chromatography; TAD, β-methylenethiazole-4-carboxamide adenine dinucleotide.

10.1021/bi034625w CCC: $25.00
Published on Web 08/09/2003

but can be released on cell damage in injured or inflamed tissues (*13*, *21*). In rat, extracellular NAD^+ blocked T cell activation and proliferation (*21*). Moreover, the absence of rART2.2-expressing T cells increased the risk of diabetes mellitus (*22*).

The variant rART2.2 is known to catalyze auto-ADP-ribosylation and NAD^+ hydrolysis (*16*, *17*, *23*, *24*). A dominance of the hydrolase over the transferase activity has been reported (*23*). However, the only reported value for the hydrolysis rate (*18*) is much lower than usual for hydrolases. Here we present the structures of complexes between wild-type and two mutant rART2.2s on one hand and the substrate analogues β-methylenethiazole-4-carboxamide adenine dinucleotide (TAD) and NADH as well as the substrate NAD^+ on the other. Moreover, we report a NAD^+ hydrolysis rate meeting that of common hydrolases, and we propose a mechanism for the hydrolysis and for the established auto-ADP-ribosylation.

MATERIALS AND METHODS

Mutagenesis, Protein Purification, and Crystal Production. The mutations were performed in the expression vector pASK60 using the PCR-based QuikChange kit (Stratagene). Primers 5′-CCG TCC TGA CCA AGA GGC GGT GTT AAT TCC AGG C-3′ for mutant E189A, 5′-CCG TCC TGA CCA AGA GTC CGT GTT AAT TCC AGG C-3′ for E189S, 5′-CCG TCC TGA CCA AGA GAT CGT GTT AAT TCC AGG CTA TGA GG-3′ for E189I, and 5′-CTC TTT CCG TCC TGA CGC AGA GGC GGT GTT AAT TCC AGG C-3′ for the double mutant Q187A-E189A together with their antisense partners were obtained from MWG-Biotech (München) or Eurogentech (Köln). All mutations were verified by DNA sequence analyses (SeqLab, Göttingen). The recombinant rART2.2 from *Rattus norvegicus* was expressed in *Escherichia coli*, purified, and crystallized as described (*25*). The yield was about 0.2 mg of rART2.2/L of culture. The inhibitor complex was produced by soaking wild-type crystals for 60 min in 60 mM TAD in buffer A [100 mM Tris, pH 8.3, 28% (w/v) PEG 4000]. The other two complexes were produced by soaking crystals of mutants E189I and E189A for 10 min in buffer A containing 50 mM NAD^+ and 50 mM NADH, respectively. After being soaked, all crystals were transferred in four steps to 20% (v/v) glycerol in buffer A, mounted on a cryo loop, and flash-frozen at 100 K.

Data Collection and Structure Analysis. X-ray data of the wild type•TAD complex crystals were collected at beamline X11 (EMBL Outstation, Hamburg), whereas the data of the other complexes were measured using a rotating anode X-ray generator (Rigaku, model RU200B) with an image plate (Marresearch, model 30 cm). All data were processed and scaled with the HKL program suite (*26*). The water- and ligand-free wild-type model (*6*) was positioned using the program MolRep-auto MR (*27*). The ligands were located using difference Fourier maps and refined with the program CNS (*28*). All manual operations were done with the program O (*29*). After the *R*-factor had dropped below 24%, water molecules were assigned with the program CNS (*28*) and also introduced manually. They were kept if their density remained above 0.7σ in the $2F_o - F_c$ map. The structure alignments were done using program LSQMAN (*30*). The figures were produced with the programs Molscript (*31*) and Raster3D (*32*). The coordinates and structure factors were deposited in the Protein Data Bank under accession codes 1OG1, 1OG3, and 1OG4.

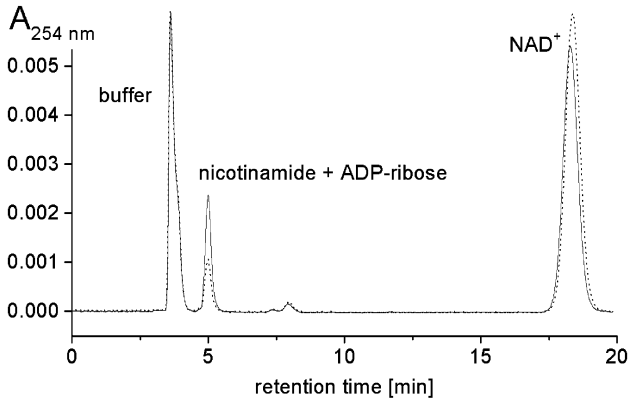

FIGURE 2: NAD^+ hydrolysis assay showing the RP-HPLC chromatogram after enzymatic catalysis (solid line) and the control without enzyme (dashed line). Peaks were calibrated with nicotinamide, ADP-ribose, and NAD^+ solutions. The peak positions of nicotinamide and ADP-ribose coincide. The example refers to the low-activity mutant E189I of rART2.2 which caused the peak of NAD^+ to drop by 48 pmol and the peak of nicotinamide plus ADP-ribose to rise by 51 pmol.

NAD^+ Hydrolysis Assay. For each wild-type rART2.2 measurement, a 50 μL vial containing NAD^+ in buffer B (50 mM Tris, pH 7.5, and 1 mM EDTA) and a given amount of the enzyme was incubated for 1 min at 37 °C and stopped by addition of 50 μL of 0.9% TFA. The solution was mixed, and a 50 μL sample was applied directly onto a RP-HPLC column (Aqua 5u C18 125 A, Phenomenex) and run under isocratic conditions at a flow rate of 1 mL/min 0.1% TFA, monitoring the absorbance at 254 nm. A control without enzyme was always analyzed in parallel. A typical chromatogram is shown in Figure 2. The NAD^+ hydrolysis rates were deduced from the decrease of the NAD^+ peak and the increase of the peak representing the sum of nicotinamide and ADP-ribose. The enzyme concentrations were determined photometrically ($\epsilon_{280} = 29540\ M^{-1}\ cm^{-1}$). NAD^+ hydrolysis of the control was below 1% per minute. About 9% of the applied NAD^+ was already hydrolyzed from the start.

The four mutants and their controls were incubated for 10 min instead of 1 min for the wild type. The incubation was stopped by addition of 450 μL of 0.1% TFA to the 50 μL reaction mixture and centrifugation. A 20 μL sample was analyzed by RP-HPLC in the same manner as in the wild-type experiments. The mutant measurements were at NAD^+ concentrations much higher than the K_M value of the wild type using also much higher enzyme concentrations. Taking K_M as the NAD^+ dissociation constant, the NAD^+ saturation of the enzyme was calculated in each case, and the rate was corrected for full substrate saturation of the enzyme; the correction always stayed below 25%.

RESULTS AND DISCUSSION

Structure Analysis. Wild-type rART2.2 has been crystallized in forms A, B, and C belonging to space groups $P2_1$, $P2_12_12_1$, and $P3_121$, respectively (*6*). Only crystal form C was easily reproducible and therefore used here. All attempts

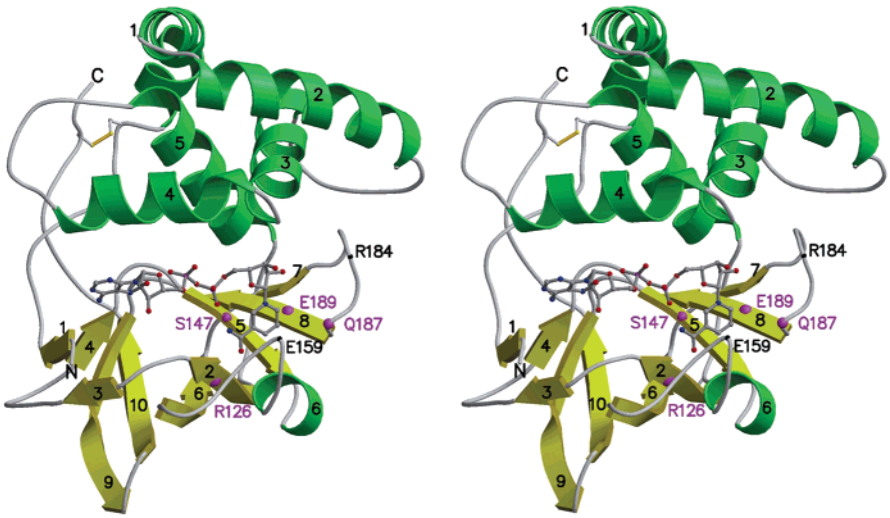

FIGURE 3: Stereo ribbon plot of rART2.2 with bound NAD^+ and labeled secondary structure elements. The native protein is located at the outside of the plasma membrane fixed by a GPI anchor at its C-terminus. The Cα atoms of R184 in the specificity-determining "ARTT" loop (*35*) and of the base E159 are marked (black). R184 is the putative auto-ADP-ribosylation site. The positions of the sequence fingerprint residues R...S...QxE (*10*) are shown in magenta.

to cocrystallize wild type or mutant rART2.2 with substrates or analogues failed. Soaking wild type crystals with 10 mM NAD^+ caused crystal damage after several minutes, indicating that a reaction takes place which involves structural changes at a packing contact. Soaking a crystal of mutant E189A with 10 mM NAD^+ for 10 min followed by flash-freezing to 100 K and structure analysis resulted in a bound nicotinamide with no density for the ADP-ribose. Obviously, the residual hydrolytic activity of E189A sufficed to split all NAD^+ in the crystal, notably without breaking it. However, this complex was not further analyzed because the nicotinamide binding site is well established (*6*, *33*, *34*).

More successful was a soaking experiment of an E189A crystal in 50 mM NADH for 10 min and subsequent flash-freezing to 100 K that showed the full substrate analogue. Moreover, the full substrate was bound in a crystal of mutant E189I after soaking with 50 mM NAD^+ for 10 min and subsequent flash-freezing to 100 K. Presumably this worked out because E189I shows four times less hydrolytic activity than E189A (see below). Finally, the substrate location was established at 2.0 Å resolution by soaking wild type rART2.2 crystals with 60 mM substrate analogue TAD for 60 min.

X-ray data of reasonable quality were collected from the crystals of the wild type·TAD, the mutant E189I·NAD^+, and the E189A·NADH complexes (Table 1). Since the crystals were isomorphous to those of ligand-free wild type rART2.2 (*6*), the structures were solved by placing the wild type model at the appropriate position and locating the ligands by difference Fourier methods. The refinements of these three structures yielded accurate models (Table 2). None of the analyses had interpretable electron density for the first three amino acid residues. The *B*-factor plots remained essentially the same as with the ligand-free enzyme (*6*). The general structure of the enzyme−substrate complex is depicted in Figure 3.

Substrate Binding Mode. The substrate NAD^+ binds in a long and deep cleft between the N-terminal α-helical moiety and the C-terminal β-sheet moiety of rART2.2 (Figure 3). This binding site is typical for all ARTs and strongly conserved (*6*, *35*). In our structures all three ligands bind in similar conformations and show essentially the same *B*-factor variation with minima at the adenine and nicotinamide moieties and maxima at the phosphates and nicotinamide ribose, the difference being about 20%. The low *B*-factor of the nicotinamide moiety agrees with the observation that NAD^+ hydrolysis in mutant E189A resulted in a fully occupied nicotinamide site. The high *B*-factors of the

Table 1: Data Collection Statistics of rART2.2 Crystals[a]

	wild type·TAD	E189I·NAD^+	E189A·NADH
unit cell			
$a = b$ (Å)	81.4	81.7	81.3
c (Å)	77.3	77.8	77.2
resolution range (Å)	20−2.0	50−2.6	50−2.6
unique reflections	20469 (698)	9591 (474)	9461 (453)
multiplicity	4.4 (4.3)	7.4 (7.5)	4.7 (4.8)
R_{sym-I} (%)	8.0 (40.4)	9.3 (42.0)	8.7 (40.2)
I/σ_I	20.3 (2.8)	21.6 (4.9)	17.4 (4.1)
completeness (%)	99.7 (100)	99.9 (100)	99.8 (100)

[a] All crystals are in form C belonging to space group $P3_121$. They are isomorphous with those of ligand-free wild type with unit cell parameters $a = b = 81.5$ Å and $c = 77.5$ Å (*6*). The values in parentheses refer to the last shell. All data were collected at 100 K.

Table 2: Refinement Statistics of rART2.2 Crystals

	wild type·TAD	E189I·NAD^+	E189A·NADH
resolution range (Å)	20−2.0	20−2.6	20−2.6
unique reflections	20352	9543	9372
protein atoms	1822	1821	1818
ligand atoms	43	44	44
ligand occupancy (%)	80	80	80
water atoms	179	154	138
average *B*-factors (Å^2)			
main chain	32.1	31.1	31.7
ligand	48.8	44.6	67.5
total	35.4	33.0	34.1
R_{cryst}	0.202	0.200	0.196
R_{free} (test set %)	0.244 (5)	0.242 (8)	0.255 (7)
rmsd bond lengths (Å)	0.014	0.007	0.006
rmsd bond angles (deg)	1.72	1.39	1.31
Ramachandran angles in			
most favored region (%)	89.9	87.9	84.4
allowed region (%)	10.1	11.6	15.6

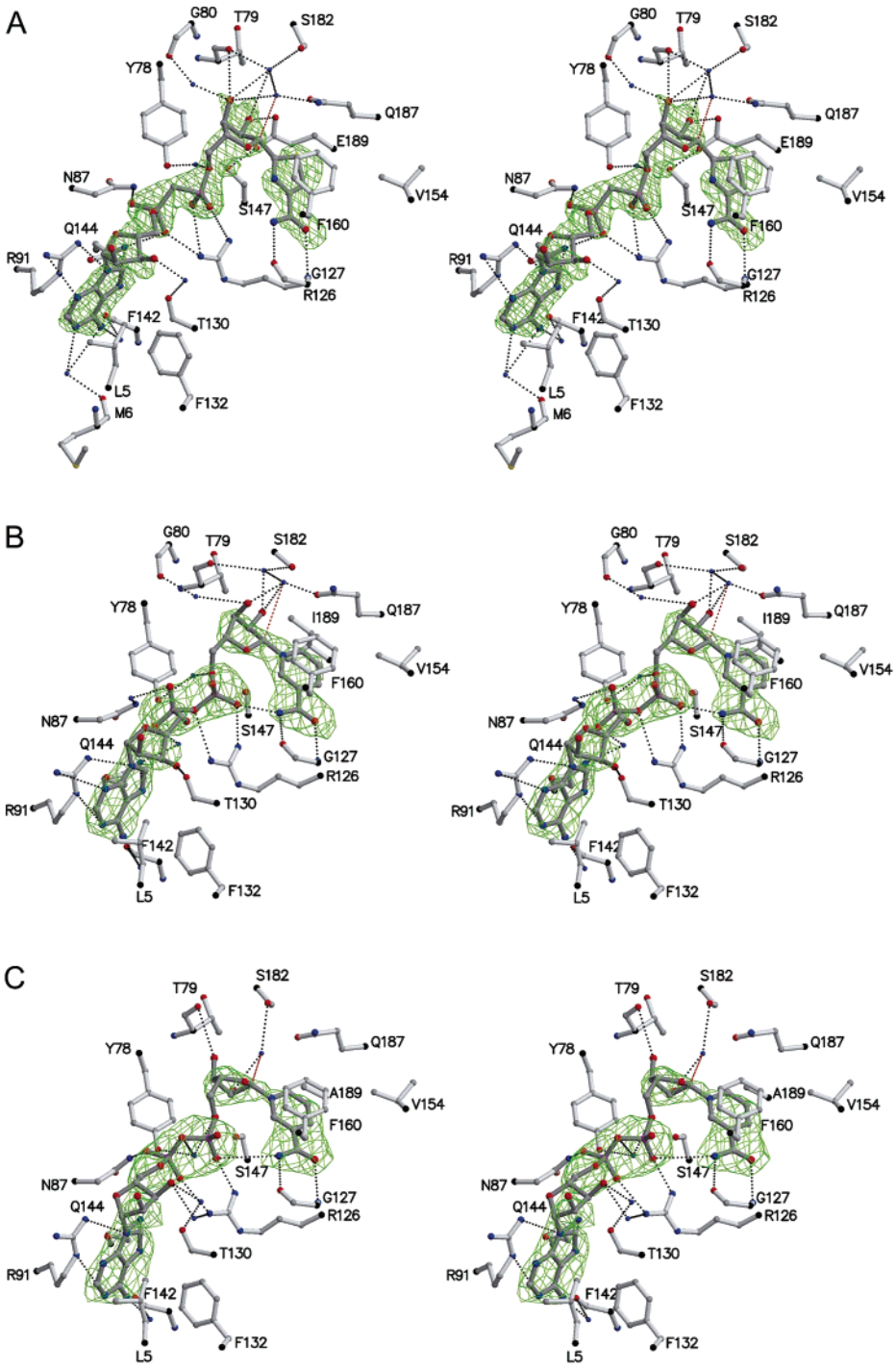

FIGURE 4: Stereo plots of the three reported complexes of rART2.2 with substrate and analogues showing the simulated annealing omit ($F_o - F_c$) electron densities. In all three cases the density distribution became continuous without being distorted at the contour levels stated below. All residues and water molecules participating in ligand binding are included. Hydrogen bonds are given by black dashed lines. Red dashed lines indicate the direction of the nucleophilic attack. Panels: (A) wild type·TAD complex with density at the 3σ contour level (continuous at 2.0σ), (B) mutant E189I·NAD^+ at 3σ (continuous at 1.9σ), and (C) E189A·NADH at 2.5σ (continuous at 1.8σ).

nicotinamide ribose reflect the required conformational change and displacement of this ribose during catalysis (*36*, *37*).

The nicotinamide is buried in a hydrophobic pocket where it undergoes $\pi-\pi$ stacking interactions with a phenylalanine (Figure 4). As in all other ARTs, the amide group forms two nearly parallel hydrogen bonds to the backbone, here at G127. The nicotinamide ribose is fixed by E189, which forms a tight hydrogen bond to the 2′-hydroxyl group and is the only residue conserved in all known ARTs. The 3′-hydroxyl of the ribose is hydrogen bonded to the carbonyl group of T79. The C1′ atom is exposed to the solvent and available for a nucleophilic attack. In the E189I·NAD^+ and E189A·NADH complexes the amide N-atom of nicotinamide forms a hydrogen bond to the proximal phosphate group, resulting in a ring within the nicotinamide moiety of NAD^+ as has been observed in other ARTs (*4*, *38*, *39*). With the analogue TAD, the five-membered thiazole ring displaces the amide, abolishing this hydrogen bond (Figure 4A). In all three complexes the pyrophosphate is bound by Y78 and N87 from

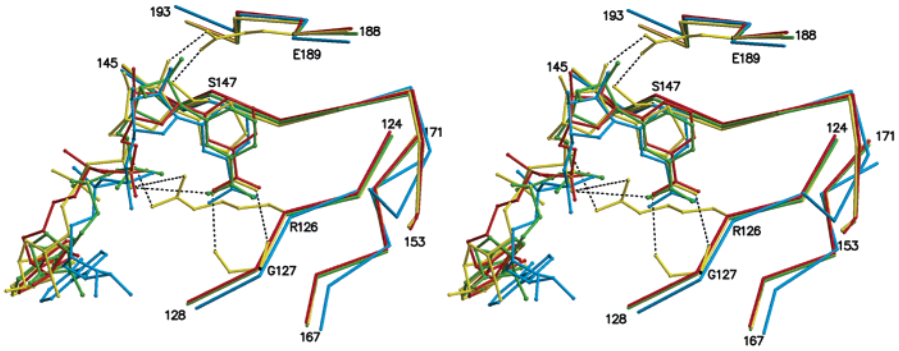

FIGURE 5: Stereoview of the three reported substrate and analogue complexes superimposed on 25 Cα positions of the four structurally highly conserved strands, β2, β5, β6, and β8, of rART2.2 (*6*) showing TAD (yellow), NAD^+ (green), and NADH (red). NAD^+ bound to exoenzyme C3 (*44*) is given in blue. The depicted sequence fingerprint residues R126, S147, and E189 (*10*) as well as G127 are involved in substrate binding and catalysis.

the α-helical moiety and by R126 from the β-sheet moiety of rART2.2. The adenine ribose forms a hydrogen bond to the Oγ atom of T130 while adenine makes $\pi-\pi$ interactions with the guanidinium group of an arginine on one side and hydrophobic interactions with a leucine on the other. Such an adenine binding site is typical for a great number of enzymes.

The deviations between the three bound substrate/analogue conformations are minor and distributed over the whole molecules (Figure 5). A comparison with NAD^+ bound to exoenzyme C3 shows that the nicotinamide half of NAD^+ superimposes better with the respective parts of the rART2.2 ligands than with the adenine half, in agreement with the larger distance of the latter from the active center. The peptide displacements on substrate binding result in an rmsd of 0.22 ± 0.03 Å for the Cα atoms when complex structures are compared with ligand-free rART2.2 (*6*). This value corresponds to the positional errors of the analyses. Remarkable movements occur in the side chains of the strongly conserved sequence fingerprint residues R...S...QxE (*10*), which are R126, S147, Q187, and E189. The guanidinium group of R126 rotates by 180° to drag the proximal phosphate into a hydrogen bond with the amide N of nicotinamide. Moreover, S147 rotates to bind to E189 as shown in Figure 4A compared to Figure 4B,C.

Kinetics of NAD^+ Hydrolysis. It was suggested that rART2.2 acts more like an NAD^+ hydrolase than an ADP-ribosyltransferase (*23*). However, the hydrolytic activity of rART2.2 was reported as 0.0044 unit/mg as determined with a radioactive assay (*18*), which is much too low for a common hydrolase. Here we determined the rate of NAD^+ hydrolysis using a novel RP-HPLC assay and obtained a specific activity of 26 units/mg, which is about 6000 times higher than the previously reported value and comparable to other hydrolases. The reported NAD^+ hydrolysis rates of other ARTs are at least 500 times lower (Table 3). The K_M value of the catalysis is 0.02 mM, which is also in the common range and in general agreement with reported values (*18*, *24*). In contrast to other data (*24*) the Lineweaver−Burk plot was linear. The high hydrolytic rate suggests that the main function of rART2.2 is the cleavage of extracellular NAD^+ arising from cell breakage.

Although all ARTs are structurally related, their sequences show remarkable variability (*10*). The only strictly conserved residue is E189 (rART2.2 numbering) that was shown to be essential for catalysis (*40*). The importance of E189 for

Table 3: Kinetic Parameters for NAD^+ Hydrolysis by rART2.2 and Four Mutants[a]

	specific activity[b] (units/mg)[d]	relative specific activity	k_{cat}[b] (s^{-1})	K_M[c] (mM)
wild type	26	100	12	0.02
E189S	0.005	0.019	0.002	
E189A	0.005	0.019	0.002	
E189I	0.0012	0.005	0.0005	
Q187A-E189A	0.0005[e]	0.002	0.0002	

[a] All data are measured at a single time point, which was 60 s for the wild type and 600 s for all mutants. A separate measurement of the wild type enzyme with 0.5 mM NAD^+ at time points 10, 20, 30, 40, 50, and 60 s showed the expected linear behavior. [b] Reported NAD^+ hydrolysis rates of other ARTs are k_{cat} = 0.021 s^{-1} for cholera toxin (*46*), 0.0083 s^{-1} for pertussis toxin (*47*), 0.0033 s^{-1} for iota toxin (*48*), 0.00012 s^{-1} for diphtheria toxin (*49*), 0.000036 s^{-1} for exoenzyme C3 (*50*), and 0.000014 s^{-1} for C2 toxin (*51*). [c] All mutants showed too low an activity to derive a K_M value. [d] 1 unit/mg is 1 μmol of reaction product per minute per milligram of enzyme. [e] The detection limit was about 0.0001 unit/mg.

NAD^+ hydrolysis was demonstrated here by replacing it by serine or alanine. Both mutants showed a 5000-fold activity decrease resulting in 0.005 unit/mg, which resembles the NAD^+ hydrolysis rates of other ARTs (Table 3). The activity decreased by a further factor of 4 when E189 was exchanged against the larger hydrophobic residue Ile that prevents a water molecule from mimicking the carboxylate, thus diminishing the transition state stabilization. This observation supports the finding that human ART3, in which E189 is replaced by an Ile, has no detectable enzymatic activity (*10*). The importance of Q187 of fingerprint R...S...QxE for NAD^+ hydrolysis was analyzed by producing the double mutant Q187A-E189A. The resulting activity was 10 times lower than that of E189A and 50000 times lower than that of the wild type, confirming that Q187 plays a role in hydrolysis. Note that all measurements were far above the detection limit of the assay (Table 3).

Catalytic Mechanism, Auto-ADP-ribosylation, and Specificity. The enzyme rART2.2 is known to catalyze NAD^+ hydrolysis and auto-ADP-ribosylation (*16*, *17*). The geometries of the two reactions are shown in panels A and B of Figure 6, which reveal the positions of the nucleophilic water molecule and of R184, respectively. The sequence fingerprint residues R...S...QxE (Figure 3) participate in the catalysis. R126 fixes the proximal phosphate in a hydrogen bond with the amide N of nicotinamide (Figure 5) that withdraws

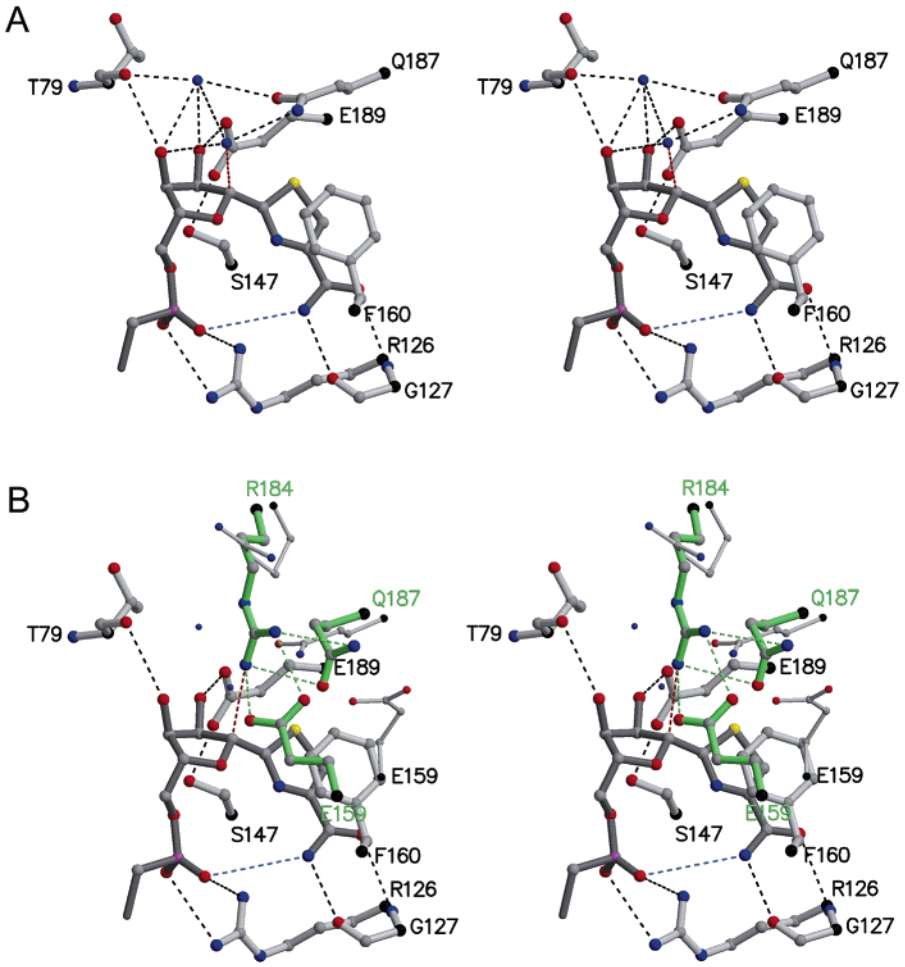

FIGURE 6: Stereoview of the active center of rART2.2. (A) Geometry of NAD^+ hydrolysis as derived from the wild type·TAD structure; the attacking water molecule at the nucleophile position, a second water, and the side chains of the R...S...QxE fingerprint and three further residues are shown (gray). Hydrogen bonds are given as black dashed lines. The ring-forming hydrogen bond between the amide and the proximal phosphate (too long in TAD) is given as a blue dashed line. The direction of the nucleophilic attack is indicated by a red dashed line. (B) Geometry of auto-ADP-ribosylation as derived from a superposition of the wild type·TAD structure (gray) with the ligand-free enzyme structure in crystal form A (*6*). Residues E159, R184, and Q187 of crystal form A are in green and are connected by green hydrogen bonds. The wild type·TAD complex in crystal form C with different packing contacts is given as a reference using thin sticks for E159, R184, and Q187. The superposition was performed on all Cα atoms.

electrons from the nicotinamide, facilitating the cleavage of the N-glycosidic bond, as has been proposed for other ARTs (*4*, *38*, *39*). This cleavage results in a positively charged oxocarbenium intermediate (*36*, *37*) which is stabilized by the negative charge at E189. A further stabilization derives from the dipoles of the hydroxyl of S147 and the carboxyl of E189, both of which contact the attacked C1′ atom (Figure 6A). S147 fixes E189 but is disoriented without its partner, as shown in the E189A and E189I mutant complexes (Figure 4). E189 forms a hydrogen bond to the 2′-hydroxyl of the ribose, polarizing the C1′−C2′ bond and thus promoting the reaction. Its importance is best demonstrated by the drastic activity decrease in the mutants of Table 3. Q187 fixes the attacking nucleophilic water molecule and is not as strictly conserved as E189, indicating lower importance. Its removal is entropically unfavorable, causing 10 times less activity (Table 3).

The auto-ADP-ribosylation is shown in Figure 6B. Since the reaction occurs on T cells (*16*, *17*), it is most likely *intra*molecular because two rART2.2 molecules GPI-anchored in the membrane should not be able to assume the relative geometry required for an *inter*molecular reaction (*6*). The reaction depends on an arginine (wild type) or a tryptophan at position 184 (*24*). In our crystal structures we find that the backbone around R184 is rather mobile so that R184 is observed in different conformations. One of these belongs to the wild type·TAD structure in crystal form C and is depicted in Figure 6B as a reference. In this conformation the guanidinium group of R184 cannot reach the attack position of the nucleophile because of steric hindrance by Q187. However, crystal form A contains a different set of packing contacts (*6*) and shows an Nη atom of R184 at the nucleophilic attack position as illustrated in green in Figure 6B. Here, Q187 has moved aside, and E159 has formed a salt bridge with R184. E159 is on the loop between helix α6 and strand β6 showing medium mobility (Figure 3) and can function as the base accepting the released proton. Since the deformation energy of crystal contacts is small, the observed R184−E159 salt bridge may also form in solution.

Together, panels A and B of Figure 6 explain the two catalytic reactions of rART2.2. The nucleophilic water (fixed by Q187) or the Nη atom of R184 (fixed by E159) attacks the C1′ atom of the ribose, and E159 functions as the base abstracting a proton from the nucleophile. The cleavage of the N-glycosidic bond results in the excellent leaving group

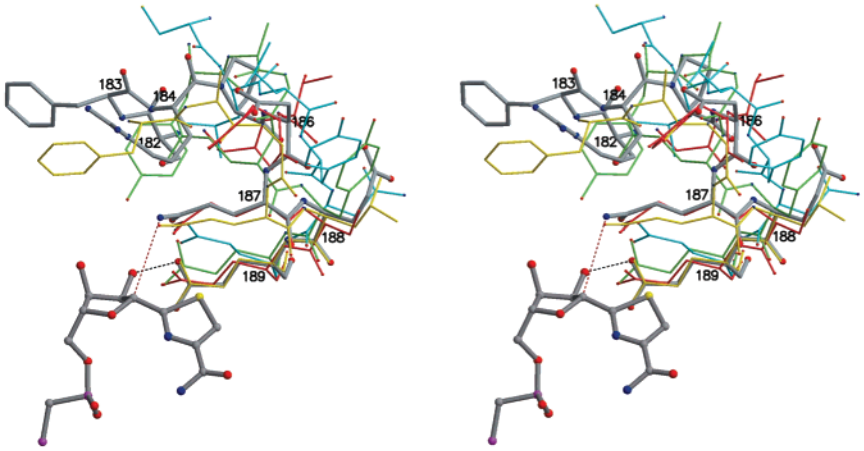

FIGURE 7: Stereoview of the specificity-determining ARTT loop (*35*) at the active center of rART2.2 (TAD complex, numbered residues SFRPDQEE, gray), with the superimposed loops of pertussis toxin (*42*) (ATYQSE, red), exoenzyme C3 (*44*) (FAGQLE, subunit A among the four subunits in the crystal, yellow), iota toxin (*4*) (YAGEYE, green), and PARP (5) (CLLYNE, blue). All structures are aligned on the 25 Cα positions of the four highly conserved β-strands of Figure 5. In rART2.2, pertussis toxin, and exoenzyme C3 the equivalent of Q187 can stabilize a water at the nucleophile position (red dashed line to the C1′ atom given as a reference).

nicotinamide and the oxocarbenium intermediate, which is stabilized by various interactions, in particular by the highly conserved E189. Figure 6B demonstrates that E159 can not only contact R184 but also reach and deprotonate the water at the nucleophilic attack position shown in Figure 6A, which may explain the high hydrolysis rate. Furthermore, Figure 6B seems to explain the auto-ADP-ribosylation of mutant R184W (*24*) because the Nϵ atom of W184 can reach a position that is only about 2 Å away from the Nη atom of R184, and such a displacement should be possible as the backbone at position 184 is highly mobile (*6*).

The structural explanation of the specificities of the ART family members is still at its infancy. Only one complex with a nucleophilic acceptor molecule is structurally elucidated (*41*). The proposed geometries for the NAD^+ hydrolysis and the auto-ADP-ribosylation of rART2.2 now add two more (comparatively simple) donor−acceptor structures. The segment between strands β7 and β8, where R184 is located (Figure 3), is an important specificity determinant and has been named the ARTT loop (*35*). In Figure 7 we have superimposed several ARTT loops to demonstrate their variance. Both E189 and residue 188 are on strand β8 and always in the same position with the same conformation. The differences start at position 187 and continue upstream. Noticeably, residue 187 of rART2.2, pertussis toxin (*42*), and exoenzyme C3 (*43*, *44*) is a glutamine that can fix a water molecule at the nucleophile attack position (Figure 7). However, such a fixation obviously does not warrant a high hydrolysis rate, because the rART2.2 rate is much higher than the rates of the other two ARTs (Table 3). Cholera toxin shows the highest hydrolysis rate besides rART2.2 (Table 3) and has a glutamate at position 187 (*45*), which may abstract a proton from a water at the nucleophile attack position. In conclusion, the reported structures and rates contribute to the elucidation of the ART specificities.

ACKNOWLEDGMENT

We thank the team of the EMBL Outstation Hamburg for help on data collection.

REFERENCES

1. Aktories, K. (1992) ADP-ribosylating toxins, Springer-Verlag, Berlin.
2. Krueger, K. M., and Barbieri, J. T. (1995) The family of bacterial ADP-ribosylating exotoxins, *Clin. Microbiol. Rev. 8*, 34−47.
3. Allured, V. S., Collier, R. J., Carroll, S. F., and McKay, D. B. (1986) Structure of exotoxin A of *Pseudomonas aeruginosa* at 3.0 Å resolution, *Proc. Natl. Acad. Sci. U.S.A. 83*, 1320−1324.
4. Tsuge, H., Nagahama, M., Nishimura, H., Hisatsune, J., Sakaguchi, Y., Itogawa, Y., Katunuma, N., and Sakurai, J. (2003) Crystal structure and site-directed mutagenesis of enzymatic components from *Clostridium perfringens* iota-toxin, *J. Mol. Biol. 325*, 471−483.
5. Ruf, A., Ménissier-de Murcia, J., de Murcia, G. M., and Schulz, G. E. (1996) Structure of the catalytic fragment of poly(ADP-ribose)polymerase from chicken, *Proc. Natl. Acad. Sci. U.S.A. 93*, 7481−7485.
6. Mueller-Dieckmann, C., Ritter, H., Haag, F., Koch-Nolte, F., and Schulz, G. E. (2002) Structure of the ecto-ADP-ribosyl transferase ART2.2 from rat, *J. Mol. Biol. 322*, 687−696.
7. Koch-Nolte, F., and Haag, F. (1997) Mono(ADP-ribosyl)transferases and related enzymes in animal tissues. Emerging gene families, *Adv. Exp. Med. Biol. 419*, 1−13.
8. Okazaki, I. J., and Moss, J. (1998) Glycosylphosphatidylinositol-anchored and secretory isoforms of mono-ADP-ribosyltransferases, *J. Biol. Chem. 273*, 23617−23620.
9. Okazaki, I. J., and Moss, J. (1999) Characterization of glycosylphosphatidylinositiol-anchored, secreted, and intracellular vertebrate mono-ADP-ribosyltransferases, *Annu. Rev. Nutr. 19*, 485−509.
10. Glowacki, G., Braren, R., Firner, K., Nissen, M., Kühl, M., Reche, P., Bazan, F., Cetkovic-Cvrlje, M., Leiter, E., Haag, F., and Koch-Nolte, F. (2002) The family of toxin-related ecto-ADP-ribosyltransferases in humans and the mouse, *Protein Sci. 11*, 1657−1670.
11. Zolkiewska, A., and Moss, J. (1995) Processing of ADP-ribosylaled integrin α7 in skeletal muscle myotubes, *J. Biol. Chem. 270*, 9227−9233.
12. Krebs, C., Koestner, W., Nissen, M., Welge, V., Parusel, I., Malavasi, F., Leiter, E. H., Santella, R. M., Haag, F., and Koch-Nolte, F. (2003) Flow cytometric and immunoblot assays for cell surface ADP-ribosylation using a monclonal antibody specific for ethenoadenosine, *Anal. Biochem. 314*, 108−115.
13. Adriouch, S., Ohlrogge, W., Haag, F., Koch-Nolte, F., and Seman, M. (2001) Rapid induction of native T cell apoptosis by ecto-nicotinamide adenine dinucleotide: requirement for mono(ADP-ribosyl)transferase 2 and a downstream effector, *J. Immunol. 167*, 196−203.

14. Liu, Z.-X., Azhipa, O., Okamoto, S., Govindarajan, S., and Dennert, G. (2001) Extracellular nicotinamide adenine dinucleotide induces T cell apoptosis in vivo and in vitro, *J. Immunol. 167*, 4942−4947.
15. Ohlrogge, W., Haag, F., Löhler, J., Seman, M., Littman, D. R., Killeen, N., and Koch-Nolte, F. (2002) Generation and characterization of ecto-ADP-ribosyltransferase ART2.1/ART2.2-deficient mice, *Mol. Cell. Biol. 22*, 7535−7542.
16. Haag, F., Andresen, V., Karsten, S., Koch-Nolte, F., and Thiele, H.-G. (1995) Both allelic forms of the rat T cell differentiation marker RT6 display nicotinamide adenine dinucleotide (NAD)-glycohydrolase activity, yet only RT6.2 is capable of automodification upon incubation with NAD, *Eur. J. Immunol. 25*, 2355−2361.
17. Rigby, M. R., Bortell, R., Stevens, L. A., Moss, J., Kanaitsuka, T., Shigeta, H., Mordes, J. P., Greiner, D. L., and Rossini, A. A. (1996) Rat RT6.2 and mouse Rt6 locus 1 are NAD^+:arginine ADP ribosyltransferases with auto-ADP ribosylation activity, *J. Immunol. 156*, 4259−4265.
18. Maehama, T., Hoshino, S., and Katada, T. (1996) Increase in ADP-ribosyltransferase activity of rat T lymphocyte alloantigen RT6.1 by a single amino acid mutation, *FEBS Lett. 388*, 189−191.
19. Hara, N., Tsuchiya, M., and Shimoyama, M. (1996) Glutamic acid 207 in rodent T-cell RT6 antigens is essential for arginine-specific ADP-ribosylation, *J. Biol. Chem. 271*, 29552−29555.
20. Karsten, S., Schröder, J., Da Silva, C., Kahlke, D., Thiele, H. G., Koch-Nolte, F., and Haag, F. (1997) Expression and comparative analysis of recombinant rat and mouse RT6 T cell mono(ADP-ribosyl)transferases in *E. coli*, *Adv. Exp. Med. Biol. 419*, 175−180.
21. Bortell, R., Moss, J., McKenna, R. C., Rigby, M. R., Niedzwiecki, D., Stevens, L. A., Patton, W. A., Mordes, J. P., Greiner, D. L., and Rossini, A. A. (2001) Nicotinamide adenine dinucleotide (NAD) and its metabolites inhibit T lymphocyte proliferation: role of cell surface NAD glycohydrolase and pyrophosphatase activities, *J. Immunol. 167*, 2049−2059.
22. Greiner, D. L., Handler, E. S., Nakano, K., Mordes, J. P., and Rossini, A. A. (1986) Absence of the RT-6 T cell subset in diabetes-prone BB/W rats, *J. Immunol. 136*, 148−151.
23. Takada, T., Iida, K., and Moss, J. (1994) Expression of NAD glycohydrolase activity by rat mammary adenocarcinoma cells transformed with rat T cell alloantigen RT6.2, *J. Biol. Chem. 269*, 9420−9423.
24. Stevens, L. A., Bourgeois, C., Bortell, R., and Moss, J. (2003) Regulatory role of arginine 204 in the catalytic activity of rat alloantigens ART2a and ART2b, *J. Biol. Chem. 278*, 19591−19596.
25. Mueller-Dieckmann, C., Scheuermann, T., Wursthorn, K., Schröder, J., Haag, F., Schulz, G. E., and Koch-Nolte, F. (2002) Expression, purification, crystallization and preliminary X-ray analysis of rat ecto-ADP-ribosyltransferase 2 (ART2.2), *Acta Crystallogr., Sect. D 58*, 1211−1213.
26. Otwinowski, Z., and Minor, W. (1997) Processing of X-ray diffraction data collected in oscillation mode, *Methods Enzymol. 276*, 307−326.
27. CCP4, Collaborative Computional Project, Number 4 (1994) The CCP4 suite: programs for protein crystallography, *Acta Crystallogr., Sect. D 50*, 760−763.
28. Brünger, A. T., Adams, P. D., Clore, G. M., DeLano, W. L., Gros, P., Grosse-Kunstleve, R. W., Jiang, J.-S., Kuszewski, J., Nilges, M., Pannu, N. S., Read, R. J., Rice, L. M., Simonson, T., and Warren, G. L. (1998) Crystallography & NMR system: A new software suite for macromolecular structure determination, *Acta Crystallogr., Sect. D 54*, 905−921.
29. Jones, T. A., Zou, J.-Y., Cowan, S. W., and Kjeldgaard, M. (1991) Improved methods for building protein models in electron density maps and the location of errors in these models, *Acta Crystallogr., Sect. A 47*, 110−119.
30. Kleywegt, G. J., and Jones, T. A. (1995) Where freedom is given, liberties are taken, *Structure 3*, 535−540.
31. Kraulis, J. (1991) MOLSCRIPT: a program to produce both detailed and schematic plots of protein structures, *J. Appl. Crystallogr. 24*, 946−950.
32. Merritt, E. A., and Bacon, D. J. (1997) Raster3D. Photorealistic molecular graphics, *Methods Enzymol. 277*, 505−524.
33. Li, M., Dyda, F., Benhar, I., Pastan, I., and Davies, D. R. (1995) The crystal structure of *Pseudomonas aeruginosa* exotoxin domain III with nicotinamide and AMP: Conformational differences with the intact exotoxin, *Proc. Natl. Acad. Sci. U.S.A. 92*, 9308−9312.
34. Ruf, A., de Murcia, G., and Schulz, G. E. (1998) Inhibitor and NAD^+ binding to poly(ADP-ribose) polymerase as derived from crystal structures and homology modeling, *Biochemistry 37*, 3893−3900.
35. Han, S., and Tainer, J. A. (2002) The ARTT motif and a unified structural understanding of substrate recognition in ADP-ribosylating bacterial toxins and eukaryotic ADP-ribosyltransferases, *Int. J. Med. Microbiol. 291*, 523−529.
36. Scheuring, J., and Schramm, V. L. (1997) Kinetic isotope effect characterization of the transition state for oxidized nicotinamide adenine dinucleotide hydrolysis by pertussis toxin, *Biochemistry 36*, 4526−4534.
37. Rising, K. A., and Schramm, V. L. (1997) Transition state analysis of NAD^+ hydrolysis by the cholera toxin catalytic subunit, *J. Am. Chem. Soc. 119*, 27−37.
38. Bell, C. E., Yeates, T. O., and Eisenberg, D. (1997) Unusual conformation of nicotinamide adenine dinucleotide (NAD) bound to diphtheria toxin: A comparison with NAD bound to the oxidoreductase enzymes, *Protein Sci. 6*, 2084−2096.
39. Han, S., Craig, J. A., Putnam, C. D., Carozzi, N. B., and Tainer, J. A. (1999) Evolution and mechanism from structures of an ADP-ribosylating toxin and NAD complex, *Nat. Struct. Biol. 6*, 932−936.
40. Carroll, S. F., and Collier, R. J. (1984) NAD binding site of diphtheria toxin: identification of a residue within the nicotinamide subsite by photochemical modification with NAD, *Proc. Natl. Acad. Sci. U.S.A. 81*, 3307−3311.
41. Ruf, A., Rolli, V., de Murcia, G., and Schulz, G. E. (1998) The mechanism of the elongation and branching reaction of poly(ADP-ribose) polymerase as derived from crystal structures and mutagenesis, *J. Mol. Biol. 278*, 57−65.
42. Stein, P. E., Boodhoo, A., Armstrong, G. D., Cockle, S. A., Klein, M. H., and Read, R. J. (1994) The crystal structure of pertussis toxin, *Structure 2*, 45−57.
43. Han, S., Arvai, A. S., Clancy, S. B., and Tainer, J. A. (2001) Crystal structure and novel recognition motif of rho ADP-ribosylating C3 exoenzyme from *Clostridium botulinum*: structural insights for recognition specificity and catalysis, *J. Mol. Biol. 305*, 95−107.
44. Ménétrey, J., Flatau, G., Stura, E. A., Charbonnier, J.-B., Gas, F., Teulon, J.-M., Le Du, M.-H., Boquet, P., and Ménez, A. (2002) NAD binding induces conformational changes in Rho ADP-ribosylating *Clostridium botulinum* C3 exoenzyme, *J. Biol. Chem. 277*, 30950−30957.
45. Zhang, R.-G., Scott, D. L., Westbrook, M. L., Nance, S., Spangler, B. D., Shipley, G. G., and Westbrook, E. M. (1995) The three-dimensional crystal structure of cholera toxin, *J. Mol. Biol. 251*, 563−573.
46. Moss, J., Stanley, S. J., and Lin, M. C. (1979) NAD glycohydrolase and ADP-ribosyltransferase activities are intrinsic to the A_1 peptide of choleragen, *J. Biol. Chem. 254*, 11993−11996.
47. Locht, C., Lobet, Y., Feron, C., Cieplak, W., and Keith, J. M. (1990) The role of cysteine 41 in the enzymatic activities of the *Pertussis* toxin S1 subunit as investigated by site-directed mutagenesis, *J. Biol. Chem. 265*, 4552−4559.
48. Nagahama, M., Sakaguchi, Y., Kobayashi, K., Ochi, S., and Sakurai, J. (2000) Characterization of the enzymatic component of *Clostridium perfringens* Iota-toxin, *J. Bacteriol. 182*, 2096−2103.
49. Blanke, S. R., Huang, K., Wilson, B. A., Papini, E., Covacci, A., and Collier, R. J. (1994) Active-site mutations of the diphtheria toxin catalytic domain: Role of histidine-21 in nicotinamide adenine dinucleotide binding and ADP-ribosylation of elongation factor 2, *Biochemistry 33*, 5155−5161.
50. Just, I., Selzer, J., Jung, M., van Damme, J., Vandekerckhove, J., and Aktories, K. (1995) Rho-ADP-ribosylating exoenzyme from *Bacillus cereus*. Purification, characterization, and identification of the NAD-binding site, *Biochemistry 34*, 334−340.
51. Barth, H., Preiss, J. C., Hofmann, F., and Aktories, K. (1998) Characterization of the catalytic site of the ADP-ribosyltransferase *Clostridium botulinum* C2 toxin by site-directed mutagenesis, *J. Biol. Chem. 273*, 29506−29511.

BI034625W